Contribution from the Department of Chemistry and Laboratory for Molecular Structure and Bonding, Texas A&M University, College Station, Texas 77843

Experimental and Theoretical Study of $Mo_2(form)_4$ and $[Mo_2(form)_4]^+$ ($form^-$ = $[(p\text{-tol})NCHN(p\text{-tol})]^-$)

F. Albert Cotton,* Xuejun Feng, and Marek Matusz

Received April 19, 1988

A new method for the preparation of $Mo_2(form)_4$, where $form^-$ = $[(p\text{-tol})NCHN(p\text{-tol})]^-$, is reported, and the conversion of this to $[Mo_2(form)_4]^+$, which was isolated as its PF_6^- salt, is described. The crystal structures of the two compounds, which were determined by X-ray crystallography, are closely related. The packing of the $Mo_2(form)_4$ units is essentially the same in each, and they crystallize in the same space group ($P4/n$) with practically the same unit cell edges. In $Mo_2(form)_4$ there are voids between the ends of adjacent molecules, whereas in the salt these voids are occupied by PF_6^- ions. The Mo–Mo distances in the molecule and the cation are 2.085 (4) and 2.122 (3) Å. Molecular orbital calculations by the SCF–SW–Xα method have been carried out on both the molecule and the cation (both spin-restricted and spin-unrestricted for the latter) and the results employed to suggest assignments of the measured electronic absorption spectra. The relationship of the small change (0.037 Å) in the Mo–Mo distance observed here to other estimates from spectroscopic measurements is discussed. The crystallographic data are as follows, where each datum is given first for the molecular compound and then for the salt: a = 13.304 (3), 13.369 (3) Å; c = 16.878 (5), 16.389 (5) Å; V = 2987 (1), 2929 (1) Å^3; Z = 2 for both.

Introduction

The existence of Mo–Mo quadruple bonds was first recognized in $Mo_2(O_2CCH_3)_4$ and other $Mo_2(O_2CR)_4$ molecules,[1] and dozens of these have been subjected to structural, spectroscopic, and theoretical study. To improve our understanding of the bonding in these molecules, several attempts have been made to study the monopositive ions that can be derived from them and to compare the parent molecules and the daughter ions. For $Mo_2(O_2CR)_4$ molecules as such, this has been somewhat frustrating because no one has yet succeeded in preparing a stable compound containing a $[Mo_2(O_2CR)_4]^+$ ion. The only information available about such ions has come from an electrochemical and EPR study of the $[Mo_2(O_2CC_3H_7)_4]^+$ ion in solution[2] and from a UPS study of the $Mo_2(O_2CCH_3)_4$ molecule and the $[Mo_2(O_2CCH_3)_4]^+$ ion obtained in the gas phase by removal of one δ electron (an ion presumed to be in the $^2B_{2g}$ state).[3]

The present work was undertaken because we reasoned that, by using a ligand that is stereoelectronically similar to a carboxyl anion but more basic, we might be able to stabilize the cation enough to isolate it in a crystalline compound. As an appropriate ligand, we selected an amidinate anion, $RNCR'NR^-$. We have previously used the one with R = p-tolyl and R' = H with success in preparing many other compounds[4,5] of the type $M_2(form)_4^n$, where n = 0, +1 and we adopt $form^-$ as a convenient way to represent the anion we are using. We therefore employed this ligand and have found that it provides the desired products.

Experimental Section

All manipulations were performed in standard Schlenkware. Di-p-tolylformamidine (Hform) was prepared according to the literature[6] and recrystallized from toluene. $AgPF_6$ was purchased from Aesar and used as received. Solvents were freshly distilled from the appropriate drying agents. Instruments used were as follows: ^1H NMR, Varian XL-200; EPR, Varian E-6S; IR, Perkin-Elmer 783; UV/vis, Cary 17; CV, BAS-100. Cyclic voltammograms were recorded in a 0.2 M solution of n-Bu_4NPF_6 in CH_2Cl_2 with a Pt disk as a working electrode and an Ag/AgCl reference electrode. Under the experimental conditions the $E_{1/2}$ for the ferrocene/ferrocenium couple was at +0.45 V.

Preparation of $Mo_2(form)_4$. Method A. Hform, 0.473 g (2.1 mmol), was dissolved in 15 mL of THF, and the solution was cooled to −78 °C. A 1.3-mL portion of a 1.6 M solution of n-BuLi in hexane was added, and the reaction mixture was allowed to warm to room temperature. This solution was transferred to a flask containing 0.22 g (0.51 mmol) of $Mo_2(O_2CCH_3)_4$. The reaction mixture was stirred and refluxed for 24 h. It was then cooled and filtered. The solid residue was washed with ether and vacuum-dried. The product was dissolved in CH_2Cl_2 to give a yellow solution, which was filtered through Celite. Partial evaporation of the solvent afforded the yellow microcrystalline product. The yield was 0.2 g (40%).

Method B. $Mo(CO)_6$, 0.8 g (3.04 mmol), Hform, 2.1 g (9 mmol), o-dichlorobenzene, 15 mL, and 2 mL of hexane were refluxed for 6 h. The reaction mixture was cooled and filtered. The solid was washed with ether and vacuum-dried. The yield was 1.55 g (94%) of canary yellow, crystalline product. $Mo_2(form)_4$ is soluble in CH_2Cl_2 and toluene but insoluble in alcohols and hexane. The density measured by flotation is 1.267 g/cm^3; calculated density (by X-ray crystallography), 1.226 g/cm^3. Anal. Calcd for $Mo_2N_8C_{60}H_{60}$: C, 66.37; H, 5.57. Found: C, 64.81; H, 5.55. ^1H NMR ($CDCl_3$): δ 2.20 s (5.56, CH_3); δ 6.075, 6.11 d (4.0, aromatic); δ 6.693, 6.733 d (4.0 aromatic); δ 8.424 s (1.1, CH). IR (Nujol, KBr plates): 1550 s, 1510 s, 1460 s, 1380 m, 1330 s, 1225 s, 1210 m, 1045 w, 940 w, 825 s, 765 w, 550 w, 520 w, 460 m cm^{-1}. UV/vis (CH_2Cl_2 solution): λ = 445 nm (sh); λ = 385 nm (sh); λ = 320 nm (sh); λ = 290 nm (ϵ = 64 600 M^{-1} cm^{-1}); λ = 270 nm (sh).

$[Mo_2(form)_4]PF_6$ (2). $Mo_2(form)_4$, 0.150 g (0.14 mmol), was dissolved in CH_2Cl_2. $AgPF_6$, 0.041 g (0.16 mmol), was dissolved in CH_2Cl_2, and the two solutions were mixed. The color changed immediately from yellow to a very dark brown, and metallic silver was precipitated. The reaction mixture was stirred for $^1/_2$ h and filtered through a short Celite column. The filtrate was layered with hexane, and after a few days a crop of black crystals was collected. The yield was 0.12 g (70%). The density measured by flotation is 1.393 g/cm^3; calculated density (by X-ray crystallography), 1.394 g/cm^3. IR (Nujol, KBr plates): 1560 s, 1540 s, 1520 s, 1470 s, 1390 m, 1330 s, 1230 s, 1200 w, 1130 w, 1050 w, 1030 w, 945 m, 880 w, 860 s, 850 s, 830 s, 750 w, 720 w, 570 w, 545 w, 520 w, 510 w, 420 m cm^{-1}. UV/vis (CH_2Cl_2): λ = 970 nm (ϵ = 260 M^{-1} cm^{-1}) (width at half-height = 3650 cm^{-1}); λ = 670 nm (ϵ = 430 M^{-1} cm^{-1}); λ = 550 nm (sh); λ = 435 nm (ϵ = 8500 M^{-1} cm^{-1}); λ = 280 nm (ϵ = 61 500 M^{-1} cm^{-1}).

X-ray Crystallography. Crystals of $Mo_2(form)_4$ were grown by layering the CH_2Cl_2 solution with hexane. Crystals grew in the form of thin plates. Crystals of $[Mo_2(form)_4]PF_6$ were obtained in the manner described above. Both were glued on top of glass fibers. Preliminary indexing revealed tetragonal cells. Axial lengths and Laue class ($4/m$) were confirmed with oscillation photographs. The space group for both compounds was uniquely determined from systematic absences as $P4/n$ (No. 85). Data sets were treated routinely.[7] Lorentz, polarization, and absorption[8] corrections based on selected ψ scans were applied. Monitoring of three standard reflections showed only random fluctuation of intensity. In the case of **1**, absorption problems were anticipated because of the platelike shape of the crystal, with the thickness of the crystal estimated at 0.02 mm or less. The data were therefore corrected with the program DIFABS.[9] Both structures refined routinely with all the

(1) Cotton, F. A.; Walton, R. A. *Multiple Bonds Between Metal Atoms*; John Wiley & Sons: New York, 1982; Chapter 3.
(2) Cotton, F. A.; Pedersen, E. *Inorg. Chem.* **1975**, *14*, 399.
(3) Lichtenberger, D. L.; Blevins, C. H., III. *J. Am. Chem. Soc.* **1984**, *106*, 1636.
(4) Cotton, F. A.; Poli, R. *Polyhedron* **1987**, *6*, 1625.
(5) Cotton, F. A.; Matusz, M.; Poli, R.; Feng, X. *J. Am. Chem. Soc.* **1988**, *110*, 1144.
(6) Roberts, R. M. *J. Org. Chem.* **1949**, *14*, 277.
(7) Calculations were done at the laboratory for Molecular Structure and Bonding on a MicroVAX II computer with SDP-plus package software.
(8) North, A. C. T.; Phillips, D. C.; Mathews, F. S. *Acta Crystallogr., Sect. A* **1968**, *A24*, 351.
(9) Walker, N.; Stuart, D. *Acta Crystallogr., Sect. A* **1983**, *A39*, 158.

0020-1669/89/1328-0594$01.50/0

Table I. Crystallographic Data for $Mo_2(form)_4$ and $Mo_2(form)_4PF_6$

formula	$Mo_2N_8C_{60}H_{60}$	$Mo_2N_8C_{60}H_{60}PF_6$
fw	1103.1	1230.05
space group	$P4/n$	$P4/n$
systematic absences	$hk0$: $h + k \neq 2n$	$hk0$: $h + k \neq 2n$
a, Å	13.304 (3)	13.369 (3)
b, Å	13.304 (3)	13.369 (3)
c, Å	16.878 (5)	16.389 (5)
α, deg	90.0	90.0
β, deg	90.0	90.0
γ, deg	90.0	90.0
V, Å^3	2987 (1)	2929 (1)
Z	2	2
d_{calc}, g/cm^3	1.226	1.394
cryst size, mm	0.2 × 0.3 × 0.02	0.3 × 0.5 × 0.15
μ(Mo Kα), cm^{-1}	4.506	5.054
data collcn instrument	AFC5R	P3
radiation (monochromated in incident beam)	Mo Kα (λ_α = 0.71073 Å)	
orientation reflcns: no.; range (2θ), deg	25; $14 < 2\theta < 25$	25; $18 < 2\theta < 30$
temp, °C	22	22
scan method	ω–2θ	ω–2θ
data collcn range (2θ), deg	4–45	4–50
no. of unique data; tot. no. with $F_o^2 > 3\sigma(F_o^2)$	1306; 761	1693; 1051
no. of params refined	160	178
rel trans factors: max; min	0.999; 0.660	0.999; 0.878
R^a	0.0746	0.0707
$R_w{}^b$	0.0911	0.0891
quality-of-fit indicator^c	1.5203	1.886
largest shift/esd, final cycle	0.18	0.22
largest peak, e/Å^3	1.16	0.874

$^a R = \sum||F_o| - |F_c||/\sum|F_o|$. $^b R_w = [\sum w(|F_o| - |F_c|)^2/\sum w|F_o|^2]^{1/2}$; $w = 1/\sigma^2(|F_o|)$. ^{c}Quality-of-fit = $[\sum w(|F_o| - |F_c|)^2/(N_{obsvns} - N_{params})]^{1/2}$.

non-hydrogen atoms anisotropic. The results of crystallographic procedures are summarized in Table I.

Computational Procedures. The SCF–Xα–SW calculations[10] were carried out for the model systems $Mo_2(HNCHNH)_4$ and $[Mo_2(HNCHNH)_4]^+$. The atomic coordinates used in the calculations were obtained from the bond distances and angles that were taken from the crystal structures of the real compounds and were idealized to D_{4h} symmetry. The bond distances used for C–H and N–H were 1.08 and 1.06 Å, respectively. The initial molecular potentials were constructed from Herman–Skillman atomic potentials[11] and H 1s radial functions. The atomic sphere radii used were 88.5% of the atomic number radii[12] for $Mo_2(HNCHNH)_4$ and 91% for $[Mo_2(HNCHNH)_4]^+$. The partial wave basis consisted of s-, p-, and d-type spherical harmonics on the Mo atoms, s and p on the C and N atoms, and s only on the H atoms and ranged up through $l = 5$ on the outer sphere.

The SCF calculation on $Mo_2(HNCHNH)_4$ was performed spin-restrictedly. The cation $[Mo_2(HNCHNH)_4]^+$ was first calculated with the spin-restricted procedure, but after convergence, the potential and energy levels were made spin-unrestricted and reconverged.

The calculations of the electronic transitions were started with the converged ground-state molecular potential, and the transition-state procedure[10a] was used. To obtain explicitly each of the singlet transition energies for $Mo_2(HNCHNH)_4$, two different spin-unrestricted calculations were performed. This gave rise to predictions of the triplet energy and the simple average of the singlet and triplet energies. The two results then were used to evaluate the required singlet energy.[13]

To test the suitability of $HNCHNH^-$ as a model for the actual formamidinium ligand, ab initio Hartree–Fock calculations were carried out on both $HNCHNH^-$ and $C_6H_5NCHNC_6H_5^-$. In each case C_{2v} symmetry was used and the latter system was made completely planar. A similar calculation was carried out on the aniline molecule employing the microwave structural data of Lister et al.[14] In all these calculations the 4-31G Gaussian basis functions of Pople and co-workers[15] were used.

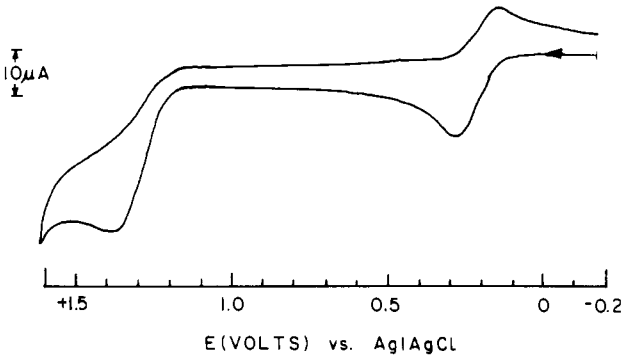

Figure 1. Cyclic voltammogram of $Mo_2(form)_4$ (scan speed 200 mV/s).

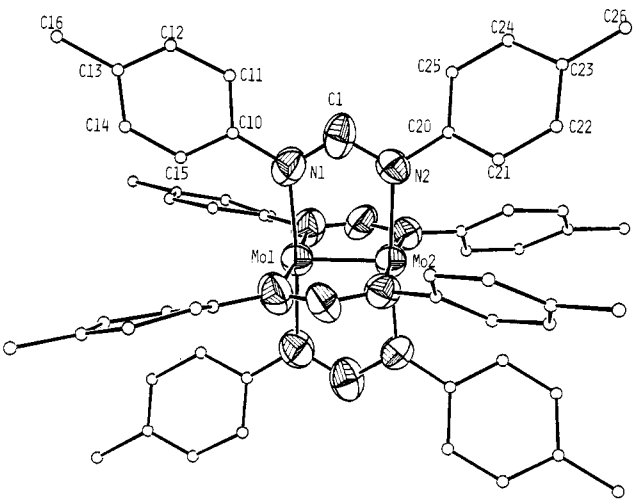

Figure 2. ORTEP drawing of the $Mo_2(form)_4$ molecule at 50% probability level. Tolyl carbons are drawn as small circles for the sake of the clarity.

Table II. Positional Parameters and Their Estimated Standard Deviations for $Mo_2(form)_4$[a]

atom	x	y	z	B, Å^2
Mo(1)	0.250	0.250	0.6768 (2)	3.71 (5)
Mo(2)	0.250	0.250	0.5533 (2)	3.46 (4)
N(1)	0.200 (1)	0.0983 (9)	0.6833 (7)	4.1 (3)
N(2)	0.207 (1)	0.089 (1)	0.5492 (7)	5.1 (3)
C(1)	0.186 (1)	0.049 (1)	0.6199 (8)	4.7 (4)
C(10)	0.176 (1)	0.048 (1)	0.7571 (9)	4.9 (5)
C(11)	0.090 (2)	−0.013 (1)	0.756 (1)	6.6 (6)
C(12)	0.059 (2)	−0.060 (2)	0.827 (1)	9.9 (8)
C(13)	0.116 (2)	−0.054 (2)	0.893 (1)	8.7 (6)
C(14)	0.200 (2)	0.008 (1)	0.889 (1)	8.1 (6)
C(15)	0.233 (1)	0.057 (2)	0.8199 (9)	6.2 (5)
C(16)	0.093 (2)	−0.100 (2)	0.972 (1)	14 (1)
C(20)	0.197 (1)	0.038 (1)	0.475 (1)	6.2 (5)
C(21)	0.272 (2)	0.060 (2)	0.414 (1)	11.7 (9)
C(22)	0.252 (2)	0.000 (2)	0.339 (1)	9.5 (7)
C(23)	0.179 (2)	−0.069 (2)	0.329 (1)	7.6 (6)
C(24)	0.121 (3)	−0.095 (2)	0.392 (1)	15 (1)
C(25)	0.113 (2)	−0.045 (2)	0.468 (2)	17 (1)
C(26)	0.166 (2)	−0.125 (2)	0.250 (1)	10.6 (8)

[a] Anisotropically refined atoms are given in the form of the isotropic equivalent thermal parameter defined as $(4/3)[a^2B(1,1) + b^2B(2,2) + c^2B(3,3) + ab(\cos\gamma)B(1,2) + ac(\cos\beta)B(1,3) + bc(\cos\alpha)B(2,3)]$.

Results and Discussion

The compound $Mo_2(form)_4$ has been prepared previously (along with several others having, e.g., phenyl, xylyl, or *o*-tolyl rings instead of *p*-tolyl rings) but only by method B.[16] There is excellent agreement between our NMR data and that previously reported.

(10) (a) Slater, J. C. *Quantum Theory of Molecules and Solids*; McGraw-Hill: New York, 1974; Vol. IV. (b) Johnson, K. H. *Adv. Quantum Chem.* **1973**, *7*, 143.
(11) Herman, F.; Skillman, S. *Atomic Structure Calculations*; Prentice-Hall: Englewood Cliffs, NJ, 1963.
(12) Norman, J. G., Jr. *Mol. Phys.* **1976**, *31*, 1191.
(13) Ziegler, T. In *Local Density Approximation in Quantum Chemistry and Solid State Physics*; Dahl, J. P., Avery, J., Eds.; Plenum Press: New York, 1984.
(14) Lister, D. G.; Tyler, J. K.; Hog, J. H.; Larsen, N. W. *J. Mol. Spectrosc.* **1973**, *48*, 86.
(15) Frisch, M. J.; Pople, J. A.; Binkley, J. S. *J. Chem. Phys.* **1984**, *80*, 3265.
(16) DeRoode, W. H.; Vrieze, K.; Koerner von Gustorf, E. A.; Ritter, A. *J. Organomet. Chem.* **1977**, *135*, 183.

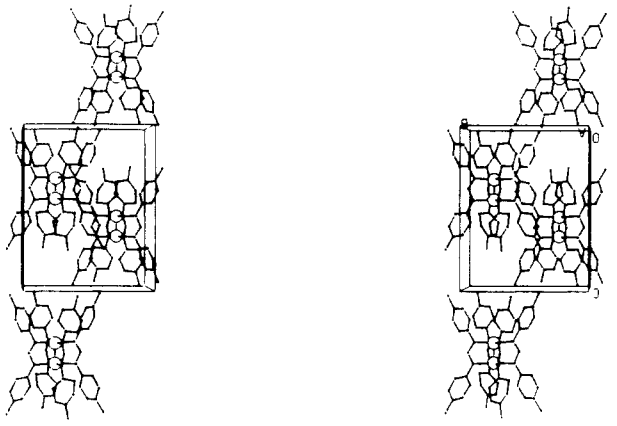

Figure 3. Packing diagram for $Mo_2(form)_4$. The view is along the *a* crystallographic axis.

Table III. Selected Bond Distances (Å) and Angles (deg) for $Mo_2(form)_4$[a]

Mo(1)–Mo(2)	2.085 (4)	N(1)–C(10)	1.45 (2)
Mo(1)–N(1)	2.126 (14)	N(2)–C(1)	1.33 (2)
Mo(2)–N(2)	2.216 (14)	N(2)–C(20)	1.44 (2)
N(1)–C(1)	1.27 (2)		
Mo(2)–Mo(1)–N(1)	92.9 (5)	Mo(2)–N(2)–C(1)	114 (1)
Mo(1)–Mo(2)–N(2)	91.8 (5)	Mo(2)–N(2)–C(20)	121 (1)
Mo(1)–N(1)–C(1)	120 (1)	C(1)–N(2)–C(20)	125 (2)
Mo(1)–N(1)–C(10)	124 (1)	N(1)–C(1)–N(2)	121 (2)
C(1)–N(1)–C(10)	117 (2)		

[a] Numbers in parentheses are estimated standard deviations in the least significant digits.

We have characterized the compound more extensively in several ways not previously used, including X-ray crystallography. This yellow, crystalline compound is stable in air. We were pleased to see that in dichloromethane solution there is a reversible oxidation (see Figure 1) at +0.21 V vs Ag/AgCl, indicating that a stable cation, $[Mo_2(form)_4]^+$, should be obtainable. By trial and error it was found that $AgPF_6$ allowed us to achieve a clean oxidation and obtain an isolable crystalline salt, $[Mo_2(form)_4]PF_6$. We were thus in a position to carry out the first detailed comparison of the structural and spectroscopic properties of a compound such as $Mo_2(form)_4$ and its +1 cation. We turn first to the structural results.

Molecular Structure of $Mo_2(form)_4$ (1). A labeled ORTEP diagram is presented in Figure 2, which also explains the labeling scheme. Atomic fractional coordinates are given in Table II. The molecule resides on a crystallographic 4-fold axis with the Mo–Mo vector aligned with it. There are two molecules in the unit cell, and a packing diagram is presented in Figure 3. The molecules form stacks along the *z* axis, and, as can be seen from the packing diagram, there are empty pockets halfway between two molecules (looking along the *z* direction). The structure of the molecule is the typical paddlewheel type, and the separation of the molybdenum atoms is 2.085 (4) Å. The crystallographically imposed symmetry is C_4, and there are two independent Mo–N distances, Mo(1)–N(1) = 2.126 (14) Å and Mo(2)–N(2) = 2.216 (14) Å, as well as a nonzero N–Mo–Mo–N torsion angle of 3.2 (5)°. The remaining distances and angles (Table III) require no comment. Some of the phenyl carbon atoms refined with unusually large thermal displacement parameters, ca. 17 Å^2 for C(25), which is indicative of a loose packing, a conclusion supported by inspection of the packing diagram.

Structure of $[Mo_2(form)_4]PF_6$ (2). Fractional coordinates are given in Table IV. There is a striking similarity between the cell dimensions of **1** and **2** (Table I). As pointed out above, there are empty pockets in the unit cell of $Mo_2(form)_4$. Inspection of the packing diagram (Figure 4) of $[Mo_2(form)_4]PF_6$ reveals that the PF_6^- anions reside there. This leads to some changes in the van der Waals contacts as the molecules are shifted on the 4-fold axis. The cell volume of the salt is slightly smaller than that for the neutral molecule, contradictory to what might have been expected on the basis of the number of atoms, but easily explainable by the fact that electrostatic interaction in the salt accounts for tighter packing. There is a virtually negligible increase in the *a* dimension of the unit cell upon introducing the PF_6^- ions (0.5%) but an appreciable (3%) contraction in the *c* dimension. The Mo–F distances are 5.537 and 5.620 Å. These very long distances rule out any significant covalent axial bonding to the molybdenum atoms. Because of the electrostatic interaction between the Mo dimer and the PF_6^- anion, the symmetry of the PF_6^- anion is distorted from that of the ideal octahedron (O_h) to that of a tetragonal bipyramid (D_{4h}). The P–F distances in the 4-fold direction are longer (1.52 (3) and 1.59 (3) Å) than the off-axis distance of 1.48 (2) Å. The tetragonal distortion from the octahedral symmetry of the PF_6^- anion must be reflected in the infrared stretching frequencies (a similar situation was encountered[5] with the $[Pd_2(form)_4]PF_6$ salt). The T_{1u} stretching vibration in an octahedral PF_6^- anion is found at 840 cm^{-1}. When the symmetry is lowered from O_h to D_{4h}, the T_{1u} vibration splits into two modes, A_{2u} and E_u. The energy of the E_u vibration with the P–F bond perpendicular to the 4-fold axis should be little affected, and indeed there is a band at 850 cm^{-1} present in the spectrum that is not present in the spectrum of the molecular compound. In the spectrum of $[Mo_2(form)_4]PF_6$ there is an additional strong

Table IV. Positional Parameters and Their Estimated Standard Deviations for $Mo_2(form)_4PF_6$[a]

atom	*x*	*y*	*z*	*B*, Å^2
Mo(1)	0.250	0.250	0.0452 (1)	4.24 (3)
Mo(2)	0.250	0.250	0.1746 (1)	4.14 (3)
N(1)	0.2094 (8)	0.0937 (7)	0.0392 (6)	5.6 (3)
N(2)	0.2023 (7)	0.0967 (6)	0.1806 (5)	4.5 (2)
C(1)	0.1907 (9)	0.046 (1)	0.1094 (7)	5.8 (3)
C(10)	0.197 (1)	0.0377 (8)	−0.0347 (7)	6.1 (4)
C(11)	0.145 (2)	−0.040 (1)	−0.040 (1)	17.7 (8)
C(12)	0.143 (2)	−0.095 (1)	−0.117 (1)	22 (1)
C(13)	0.176 (1)	−0.068 (1)	−0.1865 (9)	8.0 (4)
C(14)	0.216 (2)	0.015 (2)	−0.179 (1)	17.5 (8)
C(15)	0.229 (3)	0.065 (2)	−0.104 (1)	21 (1)
C(16)	0.165 (1)	−0.124 (1)	−0.2663 (9)	11.4 (5)
C(20)	0.1751 (9)	0.0470 (8)	0.2551 (7)	4.8 (3)
C(21)	0.231 (1)	0.0634 (9)	0.3242 (7)	5.5 (3)
C(22)	0.202 (1)	0.019 (1)	0.3985 (9)	7.5 (4)
C(23)	0.121 (1)	−0.046 (1)	0.4036 (8)	7.6 (4)
C(24)	0.066 (1)	−0.061 (1)	0.3306 (9)	8.7 (5)
C(25)	0.092 (1)	−0.016 (1)	0.2559 (8)	6.7 (4)
C(26)	0.091 (2)	−0.095 (1)	0.485 (1)	11.7 (6)
P(1)	0.250	0.250	0.6143 (9)	12.4 (3)
F(1)	0.250	0.250	0.707 (2)	26 (1)
F(2)	0.250	0.250	0.518 (2)	21.1 (7)
F(3)	0.286 (2)	0.355 (1)	0.613 (1)	26.7 (8)

[a] Anisotropically refined atoms are given in the form of the isotropic equivalent displacement parameter defined as $(4/3)[a^2B(1,1) + b^2B(2,2) + c^2B(3,3) + ab(\cos\gamma)B(1,2) + ac(\cos\beta)B(1,3) + bc(\cos\alpha)B(2,3)]$.

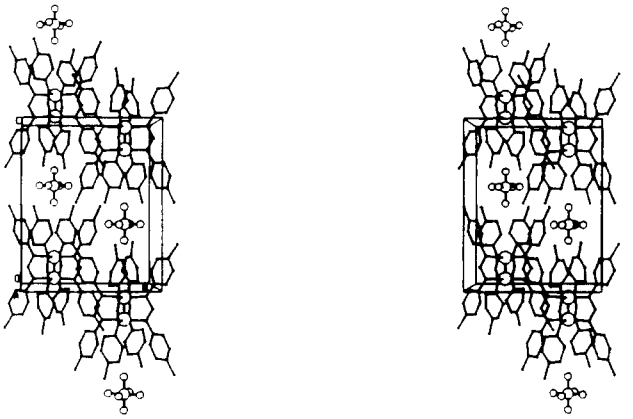

Figure 4. Packing diagram for $Mo_2(form)_4PF_6$. The view is along the *a* crystallographic axis.

Table V. Selected Bond Distances (Å) and Angles (deg) for $Mo_2(form)_4PF_6$[a]

Mo(1)–Mo(2)	2.122 (3)	N(2)–C(1)	1.358 (15)
Mo(1)–N(1)	2.161 (10)	N(2)–C(20)	1.436 (15)
Mo(2)–N(2)	2.149 (9)	P(1)–F(1)	1.52 (3)
N(1)–C(1)	1.34 (2)	P(1)–F(2)	1.59 (3)
N(1)–C(10)	1.435 (15)	P(1)–F(3)	1.48 (2)
Mo(2)–Mo(1)–N(1)	92.6 (3)	N(2)–Mo(2)–N(2)	89.9 (3)
N(1)–Mo(1)–N(1)	174.8 (4)	Mo(1)–N(1)–C(1)	117.9 (8)
N(1)–Mo(1)–N(1)	89.9 (4)	Mo(2)–N(2)–C(1)	118.0 (8)
Mo(1)–Mo(2)–N(2)	92.6 (2)	N(1)–C(1)–N(2)	119 (1)
N(2)–Mo(2)–N(2)	174.8 (4)	F(1)–P(1)–F(3)	90.7 (8)

[a] Numbers in parentheses are estimated standard deviations in the least significant digits.

band at 860 cm^{-1}. This we propose to assign to the A_{2u} mode. In the $[Pd_2(form)_4]PF_6$ compound the A_{2u} stretching frequency was found at 1160 cm^{-1}, but the distortion of the PF_6^- anion was much greater, as evidenced by much shorter Pd–F distances of 4.36 (2) Å.

The structure of the $[Mo_2(form)_4]^+$ ion (see Table V) is very similar to that of the parent molecule, with the most important difference being the longer Mo–Mo distance, 2.122 (3) Å. Again, there is only a very small internal twist, namely 2.7 (4)°. The Mo–N distances are unchanged within experimental error from those in the parent molecule and have the values 2.16 (1) and 2.15 (1) Å.

Spectroscopic Results. The electronic absorption spectra in the UV/visible region are shown in Figures 5 and 6 for $Mo_2(form)_4$ and $[Mo_2(form)_4]PF_6$, respectively. It is clear from these spectra why the colors of the compounds (yellow and black) differ so greatly. Further discussion of these spectra will be deferred until the results of the electronic structure calculations have been presented. The EPR spectrum of the $[Mo_2(form)_4]^+$ ion is shown in Figure 7. It shows much less structure than that of the $[Mo_2(O_2CC_3H_7)_4]^+$ ion,[2] and we have therefore been unable to make a meaningful assignment of spin Hamiltonian parameters, beyond the fact that the **g** tensor is approximately isotropic with a $\langle g \rangle$ value of 1.948.

Electronic Structure Calculations. $Mo_2(form)_4$. We begin with the results of the spin-restricted calculation on $Mo_2(HNCHNH)_4$ as presented in Table VI. These include the orbital energies, the relative amounts of charge in atomic spheres, and the metal angular contributions in each of the molecular orbitals listed. The HOMO is the $2b_{2g}$ orbital, which has axial δ symmetry, and the LUMO is the $2b_{1u}$ orbital, which is basically a δ^* orbital. Not listed in Table VI are the lowest lying valence levels, which are essentially unperturbed C–H, N–H and C–N σ orbitals of the ligands. Also not shown are some unoccupied valence orbitals that are very diffuse with only 2–27% of their charge located within the atomic spheres. These occur at −2.9030 eV ($4a_{2u}$), −2.3432 eV ($6a_{1g}$), −1.3359 eV ($7e_u$), −1.2302 eV ($7a_{1g}$), and −0.8950 eV ($3b_{2g}$).

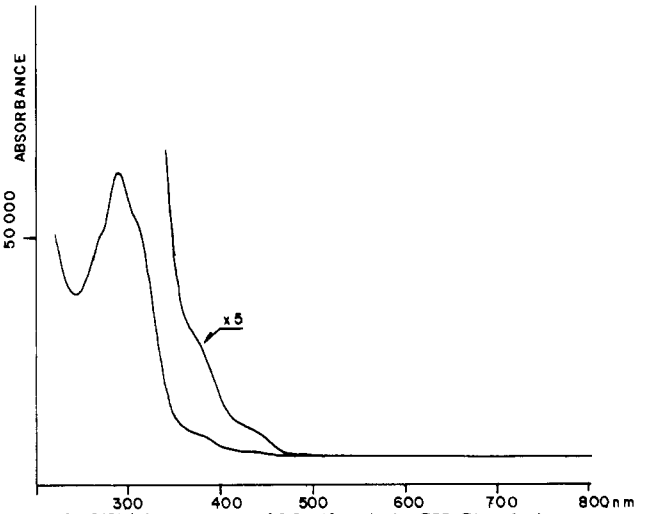

Figure 5. UV/vis spectrum of $Mo_2(form)_4$ in CH_2Cl_2 solution.

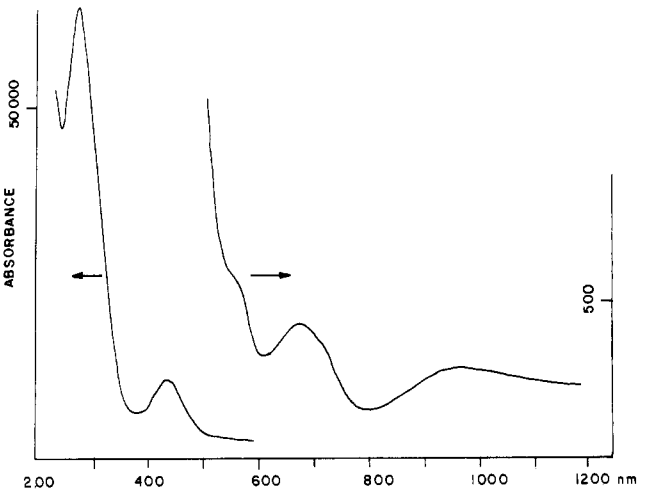

Figure 6. UV/vis spectrum of $Mo_2(form)_4PF_6$ in CH_2Cl_2 solution.

Table VI. Upper Valence Molecular Orbitals for $Mo_2(HNCHNH)_4$

D_{4h} level	energy, eV	% contribn					Mo angular contribn		
		2 Mo	8 N	4 C	8 H	4 H			
$5a_{2u}$	−0.8958	88	11	0	1	0		10% p	90% d_{z^2}
$4b_{2u}$	−1.4752	74	24	1	2	0			100% $d_{x^2-y^2}$
$5b_{1g}$	−1.5167	63	32	1	2	2			100% $d_{x^2-y^2}$
$5e_g$	−3.1620	96	3	1	0	0			100% $d_{xz,yz}$
$2b_{1u}$	−4.2015	77	23	0	0	0			100% d_{xy}
$2b_{2g}$[a]	−6.0387	87	4	9	0	0			100% d_{xy}
$1a_{1u}$	−6.2850	0	100	0	0	0			
$4e_g$	−6.7592	0	100	0	0	0			
$6e_u$	−7.9081	6	67	9	6	12			
$1b_{1u}$	−8.2154	31	69	0	0	0			100% d_{xy}
$5e_u$	−8.4123	97	1	1	1	0			100% $d_{xz,yz}$
$5a_{1g}$	−8.6737	46	35	6	4	8	47% s	5% p	48% d_{z^2}
$3e_g$	−9.2872	6	81	1	12	0			
$1a_{2g}$	−9.6375	0	67	33	0	0			
$4e_u$	−10.1103	1	68	30	0	1			
$4b_{1g}$	−10.1219	33	36	12	4	15			100% $d_{x^2-y^2}$
$3a_{2u}$	−10.6919	16	70	1	14	0	48% s		52% d_{z^2}
$4a_{1g}$	−10.9220	76	11	5	2	6	1% s	5% p	94% d_{z^2}
$1b_{2g}$	−10.9253	13	63	24	0	0			100% d_{xy}
$3b_{2u}$	−11.0815	28	59	1	12	0			100% $d_{x^2-y^2}$

[a] The highest occupied molecular orbital.

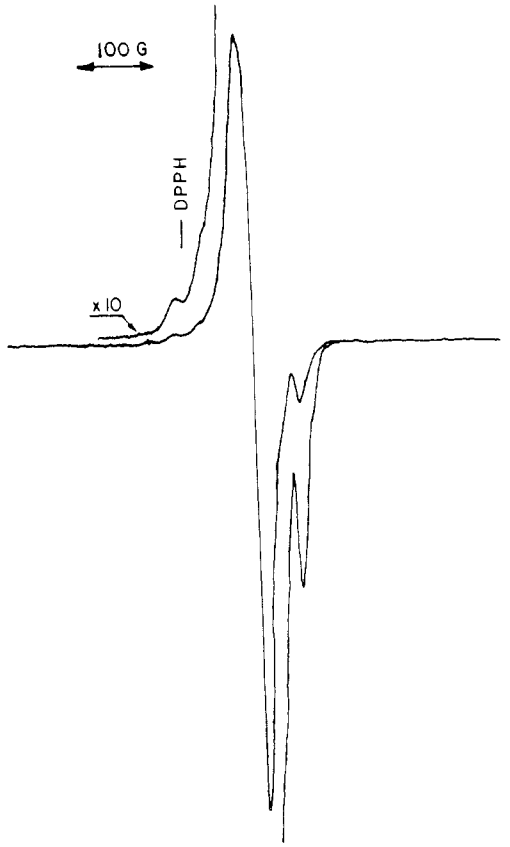

Figure 7. X-Band EPR spectrum of the CH_2Cl_2 solution of $Mo_2(form)_4PF_6$ at −196 °C.

As shown in Table VI, the basic features of the metal–metal and metal–ligand bonding in the molecule are very clear. The molecular orbitals that have dominant contributions from the metal and thus are responsible for the metal–metal bonding are the $4a_{1g}$ (σ), $5e_u$ (π), and $2b_{2g}$ (δ) orbitals. The Mo–Mo quadruple bond in the molecule is, therefore, well accounted for through the occupation of these orbitals. The ordering of the M–M bonding and antibonding molecular orbitals is as expected, namely, $\sigma < \pi < \delta < \delta^*$ ($2b_{1u}$) $< \pi^*$ ($5e_g$) $< \sigma^*$ ($5a_{2u}$), and has not been changed by the metal–ligand interactions. The metal–ligand bonding, on the other hand, is distributed over a number of molecular orbitals.

The metal–ligand σ bonding is provided mainly by the $3b_{2u}$, $3a_{2u}$, $4b_{1g}$, $3e_g$, $5a_{1g}$, and $6e_u$ orbitals, which range in energy from −11.1 to −7.9 eV and from 6 to 46% metal (average 18%). Thus, the Mo–N σ bonding can be described as moderately polar. Orbitals having mainly nitrogen σ character are $1b_{2g}$, $4e_u$, $1a_{2g}$, $1b_{1u}$, $4e_g$, and $1a_{1u}$, of which only $1b_{2g}$ and $1b_{1u}$ show much metal overlap (with d_{xy} orbitals). The remaining ones are essentially ligand-based, and the two highest, namely $1a_{1u}$ and $4e_g$, which lie just below the HOMO (δ, $2b_{2g}$), are essentially pure nitrogen lone-pair orbitals. This point will be of importance later in our discussion of the spectra.

While the overall pattern of molecular orbitals calculated for $Mo_2(HNCHNH)_4$ is similar to that previously obtained for $Mo_2(O_2CH)_4$,[17] two differences should be mentioned. The high-lying nitrogen lone-pair orbitals ($1a_{1u}$ and $4e_g$, just mentioned) are in the present case only a little below the δ orbital and well above the orbital mainly responsible for Mo–Mo π bonding ($5e_u$), whereas in the formate the $1a_{1u}$ and $4e_g$ orbitals (which are ~100% O lone pair) lie more than 0.5 eV below the Mo–Mo π orbital ($6e_u$). Another point of difference, already implicit in the preceding comment, is that the roles of the $5e_u$ and $6e_u$ orbitals are reversed in the two cases.

(17) Norman, J. G., Jr.; Kolari, H. J.; Gray, H. B.; Trogler, W. C. *Inorg. Chem.* **1977**, *16*, 987.

Table VII. Calculated and Experimental Transition Energies (cm^{-1}) for $Mo_2(form)_4$[a]

orbital transitn	type	dipole[b]	calcd	exptl[c]
$2b_{2g} \rightarrow 2b_{1u}$	$\delta \rightarrow \delta^*$	A, z	16870	22470 (445) (sh)
$4e_g \rightarrow 2b_{1u}$	$N \rightarrow \delta^*$	A, xy	23690	25970 (385) (sh)
$2b_{2g} \rightarrow 5e_g$	$\delta \rightarrow \pi^*$	F	25800	
$1a_{1u} \rightarrow 5e_g$	$N \rightarrow \pi^*$	A, xy	29110	31250 (320) (sh)
$6e_u \rightarrow 5e_g$	$N \rightarrow \pi^*$	A, z	41890	34480 (290)
				37040 (270) (sh)
$3e_g \rightarrow 2b_{1u}$	$N \rightarrow \delta^*$	A, xy	43860	
$5e_u \rightarrow 5e_g$	$\pi \rightarrow \pi^*$	A, z	45210	

[a] Calculated values are singlet transitions for $Mo_2(HNCHNH)_4$. [b] A = electric dipole allowed transition under D_{4h} symmetry; F = electric dipole forbidden transition under D_{4h} symmetry. [c] Values in parentheses have nanometer units; sh = shoulder.

Let us now turn to discussion of the electronic absorption spectrum of $Mo_2(form)_4$. The transition energies both from the calculations and from the experiment are listed in Table VII, and the calculated values are ordered to coincide with their assigned experimental transitions. It should be mentioned that the calculated transition energies are obtained for the model system in which the formamidinate ligands in the real molecule have been replaced with the $(HNCHNH)^-$ groups.

The lowest calculated transition is $2b_{2g} \rightarrow 2b_{1u}$ ($\delta \rightarrow \delta^*$) at 16870 cm^{-1}. The first transition seen in the spectrum of $Mo_2(form)_4$ is a weak shoulder at 22470 cm^{-1}, and as shown in Table VII, it is assigned as the dipole-allowed and orbitally localized $\delta \rightarrow \delta^*$ excitation. It has long been known[18] that the Xα–SW calculation always predicts too low an energy for the $\delta^2 \rightarrow \delta\delta^*$ transition in the quadruply bonded systems, because the one-electron molecular orbital formalism of the method fails to account directly for the electron correlation effects. The discrepancy between the calculated and observed $\delta \rightarrow \delta^*$ transition energies for $Mo_2(form)_4$ is typical and is of the expected magnitude. The next absorption seen in the spectrum is also a shoulder, but with increased intensity, at 25970 cm^{-1}. Although the position of the calculated forbidden $2b_{2g} \rightarrow 5e_g$ ($\delta \rightarrow \pi^*$) transition agrees well with the position of this shoulder, we prefer to assign this second absorption as the allowed charge-transfer transition, $4e_g \rightarrow 2b_{1u}$ ($N \rightarrow \delta^*$). For the shoulder at 31250 cm^{-1} we suggest assignment as the allowed $1a_{1u} \rightarrow 5e_g$ transition, which also has the nature of charge transfer from the nitrogen atoms to the metals. The calculated value for this transition is lower than the observed energy, but the agreement is still reasonable.

We now have two absorptions in the spectrum left to be assigned, namely, a very intense peak at 34480 cm^{-1} and a shoulder at 37040 cm^{-1}. Assignment of these absorptions is problematical. It is well-known that the lowest absorption band involving π-electron transitions in the benzene molecule occurs at about 38500 cm^{-1}, i.e., very close to the highest observed transition in $Mo_2(form)_4$. Therefore, the shoulder at 37040 cm^{-1} may appear in the spectrum due to a transition in the tolyl groups in the formamidinate ligands. For the intense peak we tentatively suggest assignment to the transition $6e_u \rightarrow 5e_g$ ($N \rightarrow \pi^*$). As can be seen in Table VII, the calculated energy of the transition is significantly higher than the observed value. However, the high intensity of the peak suggests that the related transition should be strongly dipole-allowed and should probably correspond to a ligand–metal charge transfer. Both of these aspects are satisfied by the $6e_u \rightarrow 5e_g$ assignment.

$[Mo_2(HNCHNH)_4]^+$. Both spin-restricted and unrestricted Xα–SW results for $[Mo_2(HNCHNH)_4]^+$ are presented in Figure 8 and compared to those for $Mo_2(HNCHNH)_4$. As can be seen in the figure, oxidation of the neutral molecule causes removal of an electron from a molecular orbital localized on the metal, namely, the $2b_{2g}$ or δ orbital. This, therefore, provides at least

(18) (a) Cotton, F. A. *Pure Appl. Chem.* **1980**, *52*, 2331. (b) Reference 1, p 390 ff. (c) Hopkins, M. D.; Gray, H. B.; Miskowski, V. M. *Polyhedron* **1987**, *6*, 705.

a qualitative explanation for the longer Mo–Mo bond distance in the oxidized species $[Mo_2(form)_4]^+$. The removal of the electron causes no reorganization or major change in the bonding character for any of the levels when compared with the case of $Mo_2(HNCHNH)_4$. In general, levels with large metal contributions have shifted down in energy more than those that are primarily ligand-based. Thus, the $4a_{1g}$ Mo–Mo σ-bonding orbital shows a very large drop, and the Mo–Mo σ-antibonding orbital changes its position from the $5a_{2u}$ orbital in the neutral molecule to the $4a_{2u}$ orbital in the cation. On the other hand, the $2b_{2g}$ and $2b_{1u}$ orbitals are not stabilized to any greater extent than some ligand-based MO's. This probably reflects the fact that the δ and δ^* orbitals are more involved in metal–ligand bonding than are the σ and π orbitals that are of mainly metal–metal character. The change in the effective oxidation state of the Mo atoms, which lowers the "empty" $d_{x^2-y^2}$ orbitals, also leads to an increased metal–ligand bonding interaction. This is indicated clearly by the relatively large drop of the $4b_{1g}$ and $3b_{2u}$ orbitals, which are both Mo–L bonding orbitals, whereas their antibonding counterparts, the $5b_{1g}$ and $4b_{2u}$ orbitals, are shifted down much less.

The calculated transition energies for $[Mo_2(HNCHNH)_4]^+$ and the experimental results for $[Mo_2(form)_4]^+$ are listed in Table VIII. Before we discuss specific assignments for the experimental transitions, it is interesting to note that the electronic absorption spectrum of $[Mo_2(form)_4]^+$ is quite different from that of the neutral compound, corresponding to the color change from yellow to black. The differences, however, may be understood in terms of the electronic structure of the compounds. As mentioned before, the σ^* orbital experiences a very large drop in the cation. This may bring some excitations to this orbital into the accessible part of the UV spectrum. In addition, the hole in the δ orbital obviously gives rise to more possibilities of electronic excitation. Consequently, as we shall see below, some absorptions in the spectrum of the cation are assigned to the transitions that are impossible or lie out of range in $Mo_2(HNCHNH)_4$.

The lowest energy absorption in the spectrum of $[Mo_2(form)_4]^+$ occurring at 10 310 cm^{-1} is very weak and is tentatively assigned as the dipole-forbidden transition $4e_g \rightarrow 2b_{2g}$ ($N \rightarrow \delta$). The transition that might occur with the lowest energy is $1a_{1u} \rightarrow 2b_{2g}$ (see Figure 8). However, its transition energy is obviously too low to be considered. The second observed absorption has been assigned as the allowed $2b_{2g} \rightarrow 2b_{1u}$ ($\delta \rightarrow \delta^*$) transition. The calculated value for the transition agrees well with the observed result, and the spin-unrestricted calculation shows an even better agreement (14 900 vs 14 930 cm^{-1} observed). This is an expected result, since the transition may be regarded as occurring in an effective one-electron system, and no correlation problem exists. The next absorption is a shoulder at 18 180 cm^{-1} and is assigned as the allowed $6e_u \rightarrow 2b_{2g}$ ($N \rightarrow \delta$) transition on the basis of the good agreement between the calculated and the experimental values. The strong absorptions at 22 990 and 35 710 cm^{-1} can reasonably be assigned as the allowed $4e_g \rightarrow 2b_{1u}$ and $4e_g \rightarrow 4a_{2u}$ transitions, respectively. Both transitions correspond to charge transfer from the N atoms to the metals and are expected to have high intensity.

Mo–Mo Bond Lengths. Our interest in how the Mo–Mo bond length would change upon oxidizing an Mo_2^{4+} complex to an Mo_2^{5+} complex was one of the main motivations for undertaking this work. It is therefore fitting to conclude the paper by discussing this point. The change we have observed is 0.037 (5) Å; if we assume that the actual value might lie within an overall range of $\pm 3\sigma$, the actual increase might be in the range 0.022–0.052 Å. Let us see how this result compares with previous ones for the $Mo_2^{4+} \rightarrow Mo_2^{5+}$ process.

The first such case to be studied was provided by the $[Mo_2(SO_4)_4]^{4-} \rightarrow [Mo_2(SO_4)_4]^{3-}$ oxidation, and in the two compounds of these ions that were first structurally characterized[19] the increase in the Mo–Mo bond length was 0.056 (2) Å. Subsequently, two other compounds of the $[Mo_2(SO_4)_4]^{3-}$ ion have been structurally characterized[20] and found to have Mo–Mo distances that are equal, within the esd's, to that found in the first one.

There is, in fact, no other prior case in which the bond lengthening effect of an $Mo_2^{4+} \rightarrow Mo_2^{5+}$ oxidation has been determined by X-ray crystallography. The one reported here is only the second one, and it entails what appears to be a somewhat smaller effect, even when the esd's are taken into account. The smaller change can be rationalized in a very natural way by noting that the basicity of the form$^-$ ligand is far greater than that of the SO_4^{2-} ligand. It was pointed out several years ago[21] that the increase in positive charge on the metal atoms would of itself contribute to weakening the metal–metal bond by causing the d orbitals to contract and overlap less well in the σ and π components of the bond. A more basic set of ligands might be expected to moderate that effect.

The idea that the form$^-$ ligand has a smaller bite than the SO_4^{2-} ligand and that this might substantially oppose and limit the increase in the Mo–Mo distance does not seem to us to have merit. In view of our recent study[22] of the $Ru_2(RNNNR)_4$ molecule, where the presence of a $\sigma^2\pi^4\delta^2\pi^{*4}$ configuration would lead one to expect a long Ru–Ru distance and where we find the actual distance to be 2.417 (2) Å, we conclude that a ligand of the form$^-$ (or very similar RCO_2^- or $RNNNR^-$) type does not effectively constrain the M–M distance. If the Mo–Mo distance would naturally tend toward a value of ca. 2.20 Å, we do not believe that the form$^-$ ligand would prevent it from becoming this long.

There are several studies that have provided indirect information on increases in the Mo–Mo bond length that result from weakening the δ component of the bond. From a study of Mo–Mo bond lengths as a function of the degree of rotation about the bond in molecules of the $Mo_2X_4P_4$ type (where P represents a phosphine or half of a diphosphine), it was concluded[23] that complete loss of the δ bond should cause the Mo–Mo distance to increase by 0.097 Å. This result is reasonably consistent with the increases we have just discussed of 0.037 and 0.056 Å, observed upon ionization, provided the charge effect is not very important. By Franck–Condon analysis of the vibrational structure of the $\delta \rightarrow \delta^*$ ($^1A_{1g} \rightarrow {}^1A_{2u}$) transition in $Mo_2(O_2CCH_3)_4$, $Mo_2[(CH_2)_2P(CH_3)_2]_4$, and a few other molecules,[24,25] the estimates of increase are in the range 0.08–0.11 Å. Here again, we are talking about complete abolition of the δ bond, so that for the removal of only one δ electron a change of half this magnitude, i.e., 0.04–0.06 Å, might be expected (again ignoring the charge effect).

The one remaining source of indirect information on this question gives a result that is somewhat out of line with the body of results just reviewed. From a Franck–Condon analysis of the vibrational structure[25] observed on the $Mo_2(O_2CCH_3)_4^+$ ion generated by photoionization of $Mo_2(O_2CCH_3)_4$, even after approximate correction for the effects of thermal vibrational excitation in the ground state,[26] the increase in the bond length in the ion appears to be 0.11 Å for loss of half the δ bond. This is 2–3 times the change we would have expected from the X-ray crystallographic results. We are unable to propose an explanation for this. It would, of course, be desirable to have both UPS and crystallographic data on the same system, and we are making an effort to find a suitable one.

Finally, we address a question raised by a reviewer of this paper concerning the suitability of $HNCHNH^-$ as a model for the real ligand. The latter has *p*-tolyl groups, whose π systems are capable of interaction with the central N–C–N π system, on the nitrogen

(19) Cotton, F. A.; Frenz, B. A.; Pedersen, E.; Webb, T. R. *Inorg. Chem.* **1975**, *14*, 391.

(20) (a) Bino, A.; Cotton, F. A. *Inorg. Chem.* **1979**, *18*, 1159. (b) Bino, A.; Cotton, F. A.; Marler, D. O.; Farquharson, S.; Hutchinson, B.; Spencer, B.; Kincaid, J. *Inorg. Chim. Acta* **1987**, *133*, 295.

(21) Cotton, F. A. *Chem. Soc. Rev.* **1983**, *12*, 35.

(22) Cotton, F. A.; Matusz, M. *J. Am. Chem. Soc.* **1988**, *110*, 5761.

(23) Campbell, F. L., III; Cotton, F. A.; Powell, G. L. *Inorg. Chem.* **1985**, *24*, 4384.

(24) Martin, D. S.; Newman, R. A.; Fanwick, P. E. *Inorg. Chem.* **1979**, *18*, 2511.

(25) Trogler, W. C.; Solomon, E. I.; Trajberg, I.; Ballhausen, C. J.; Gray, H. B. *Inorg. Chem.* **1977**, *16*, 828.

(26) Miskowski, V. M.; Brinza, D. E. *J. Am. Chem. Soc.* **1986**, *108*, 8296.

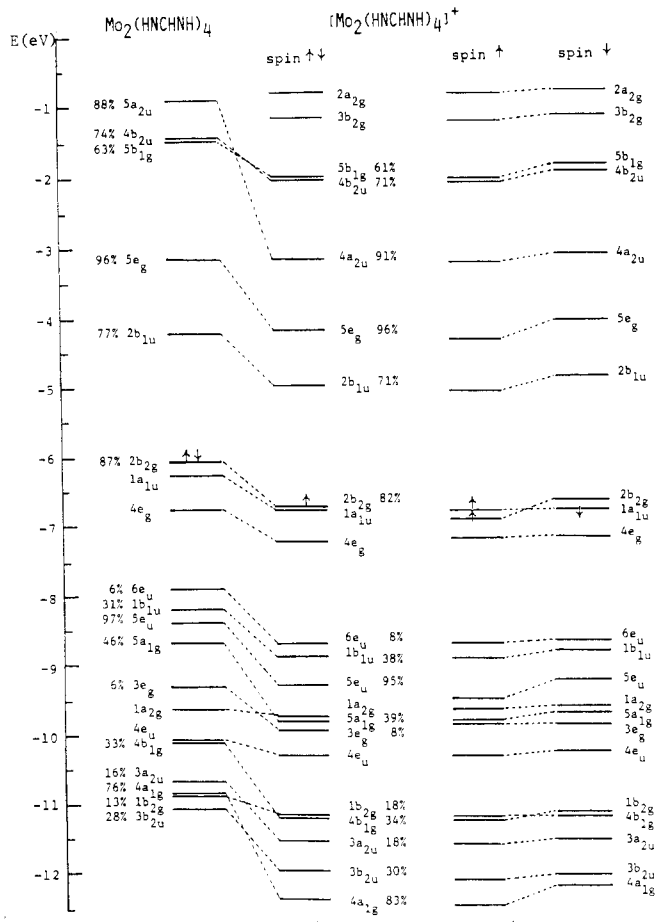

Figure 8. Energy level diagram for $[Mo_2(HNCHNH)_4]^+$ and comparison with that for $Mo_2(HNCHNH)_4$. The metal contributions in the spin-unrestricted calculation are much the same as in the spin-restricted case, and the levels in each case have been shifted up by 3 eV in drawing the diagram.

Table VIII. Calculated and Experimental Transition Energies (cm^{-1}) for $[Mo_2(form)_4]^+$

orbital[a] transitn	type	dipole	calcd[b]	exptl[c]
$4e_g \rightarrow 2b_{2g}$	$N \rightarrow \delta$	F	7170	10410 (960)
$2b_{2g} \rightarrow 2b_{1u}$	$\delta \rightarrow \delta^*$	A, z	14780	14930 (670)
$6e_u \rightarrow 2b_{2g}$	$N \rightarrow \delta$	A, xy	18380	18180 (550) (sh)
$5e_u \rightarrow 2b_{2g}$	$\pi \rightarrow \delta$	A, xy	20790	
$2b_{2g} \rightarrow 5e_g$	$\delta \rightarrow \pi^*$	F	21210	
$4e_g \rightarrow 2b_{1u}$	$N \rightarrow \delta^*$	A, xy	21380	22990 (435)
$1a_{1u} \rightarrow 5e_g$	$N \rightarrow \pi^*$	A, xy	26270	
$2b_{2g} \rightarrow 4a_{2u}$	$\delta \rightarrow \sigma^*$	F	30110	
$4e_g \rightarrow 4a_{2u}$	$N \rightarrow \sigma^*$	A, xy	34720	35710 (280)
$6e_u \rightarrow 5e_g$	$N \rightarrow \pi^*$	A, z	40600	
$5e_u \rightarrow 5e_g$	$\pi \rightarrow \pi^*$	A, z	41660	
$3e_g \rightarrow 2b_{1u}$	$N \rightarrow \delta^*$	A, xy	42890	
$3e_g \rightarrow 4a_{2u}$	$N \rightarrow \sigma^*$	A, xy	59200	

[a] The ground state of the cation is $^2B_{2g}$. [b] Results are from spin-restricted transition-state calculations for $[Mo_2(HNCHNH)_4]^+$. [c] Values in parentheses have nanometer units; sh = shoulder.

atoms. The reviewer pointed out that it is known[27,28] that a phenyl group (or, equally, a tolyl group) interacts strongly with the pπ orbital of the nitrogen atom in a molecule such as aniline. This results in a HOMO that has primarily phenyl π character rather than the nitrogen pπ character. Similar interactions might also be expected in $Mo_2(form)_4$, since the tolyl groups are far from orthogonal to the NCHN group of the form$^-$ ligand. It might then be further argued that such interactions would mix the $1a_{1u}$ and $4e_g$ orbitals (see Table VI) with some π character of the tolyl groups and might produce a HOMO that is more ligand-based than is the $2b_{2g}$ orbital in Table VI. The $2b_{2g}$ orbital might also have more ligand character due to such interactions.

To determine whether interactions of this type would be severe enough to affect the validity of our molecular orbital studies of the model system, we carried out ab initio Hartree–Fock calculations on the model ligand $(HNCHNH)^-$ and a system that should be close enough to but simpler than the form$^-$ ligand, namely, $(C_6H_5NCHNC_6H_5)^-$. In addition, the same calculation also was done for the aniline molecule for the purpose of comparison.

The calculations on $(HNCHNH)^-$ and $(C_6H_5NCHNC_6H_5)^-$ both led to a singlet ground state. For the model ligand $(HNCHNH)^-$, two orbitals of π-type were obtained, namely the $1b_1$ and $1a_2$ orbitals. The $1a_2$ orbital, which is the HOMO in the ligand, is simply a linear combination of the pπ AO's of the nitrogen atoms. For four such ligands arranged to form $Mo_2(HNCHNH)_4$ in D_{4h} symmetry, the a_2-type ligand orbitals will give rise to MO's with a_{1u}, e_g, and b_{1u} symmetries. As shown in Table VI, one has the $1a_{1u}$ and $4e_g$ orbitals, which still possess the nitrogen pπ lone-pair character. Since the ligand b_{1u} orbital has the same symmetry as the metal–metal δ^* orbital, the interaction between them results in the $1b_{1u}$ and $2b_{1u}$ orbitals. The $1b_{1u}$ orbital is then much lower in energy than the $1a_{1u}$ and $4e_g$ orbitals but has predominant nitrogen character. On the other hand, the $1b_1$ orbital of the model ligand is just the π orbital delocalized on the NCN framework. The orbitals of this type contribute to the $1a_{2g}$, $4e_u$, and $1b_{2g}$ orbitals (Table VI). Similarly, due to the interaction with the metal–metal δ orbital, the $1b_{2g}$ orbital has been mixed with a small amount of metal character and is lower in energy than the other two; the $2b_{2g}$ orbital, on the other hand, is predominantly the metal–metal δ orbital.

When the $(C_6H_5NCHNC_6H_5)^-$ ligand is considered, it is expected that both $1b_1$ and $1a_2$ orbitals of the model ligand will interact with the π orbitals of the phenyl groups. Thus, we have in total eight π-type orbitals in $(C_6H_5NCHNC_6H_5)^-$. One of the most notable features of the π-orbital diagram is the dominant character of the $1a_2$ orbital of the model ligand in the $4a_2$ orbital, which is also the HOMO in $(C_6H_5NCHNC_6H_5)^-$. Mulliken population analysis shows that the nitrogen atom character in the $4a_2$ orbital remains as high as 60%. The result is, therefore, very different from the case in molecules like aniline. Our calculation for the aniline molecule produced the same results as those in ref 27, in which the HOMO (the $3b_1$ orbital) is primarily a π orbital of the phenyl group in character and has only 20% nitrogen character.

It is important to note that the $4a_2$ orbital in $(C_6H_5NCHNC_6H_5)^-$ is energetically lower than the $1a_2$ orbital in $(HNCHNH)^-$. Thus, considering the position of the $1a_2$ orbital in the MO diagram of $Mo_2(HNCHNH)_4$, the interactions of the tolyl groups with the nitrogen atoms cannot produce a HOMO that is ligand-based in $Mo_2(form)_4$. An orbital with character similar to that of the $2b_{2g}$ orbital in $Mo_2(HNCHNH)_4$ will be still the HOMO even when the interactions with the rings are considered and included in the calculations. In addition, it must also be noted that such an orbital cannot have more ligand character than it has in $Mo_2(HNCHNH)_4$. The calculation on $(C_6H_5NCHNC_6H_5)^-$ indicates that the $2b_1$ orbital, the orbital which has primarily NCN π character, also has lower energy than the orbital of the same type, the $1b_1$ orbital, in $(HNCHNH)^-$. Thus, the interaction of the orbital of this type with the metal–metal δ orbital in the actual case cannot be stronger than the similar interaction predicted by the calculation for the model molecule $Mo_2(NHCHNH)_4$.

It should be recalled that the $(C_6H_5NCHNC_6H_5)^-$ ligand was assumed to be planar in the calculation. In the actual case, with the form$^-$ ligand departing from the planar structure, the π interactions in it will be weaker. Thus, we conclude that the

(27) Kimura, K.; Katsumata, S.; Achiba, Y.; Yamazaki, T.; Iwata, S. *Handbook of HeI Photoelectron Spectra of Fundamental Organic Molecules*; Halsted Press: New York, 1981.
(28) Debies, T. P.; Rabalais, J. W. *J. Electron Spectrosc. Relat. Phenom.* **1972/73**, *1*, 355.

modeling of the form$^-$ ligands with the $(NHCHNH)^-$ systems is a satisfactory approximation.

Acknowledgment. We thank the National Science Foundation for support.

Supplementary Material Available: Full listings of bond distances, bond angles, and anisotropic displacement parameters for $Mo_2(form)_4$ and $Mo_2(form)_4PF_6$ (4 pages); listings of observed and calculated structure factors for the complexes (10 pages). Ordering information is given on any current masthead page.

Contribution from the Department of Chemistry, Washington State University, Pullman, Washington 99164-4630

Electron Self-Exchange of Hexakis(2,6-diisopropylphenyl isocyanide)chromium(0,I) in Dichloromethane

Kim A. Anderson and Scot Wherland*

Received August 8, 1988

The rate of electron self-exchange between chromium hexakis(2,6-diisopropylphenyl isocyanide) ($Cr(CNdipp)_6$) and $Cr(CNdipp)_6BF_4$ has been measured as a function of reactant concentration and temperature, −89 to +22 °C, in CD_2Cl_2, by ^1H NMR line broadening. The temperature dependence yields an enthalpy of activation of 1.5 ± 0.2 kcal/mol and an entropy of activation of −15.6 ± 0.6 cal/(mol K). These extrapolate to a rate constant of 1.8×10^8 M^{-1} s^{-1} at 25 °C, one of the highest electron self-exchange rate constants known.

Introduction

Outer-sphere electron-transfer reactions have been the subject of extensive experimental and theoretical study.[1-3] Electron self-exchange reactions have been of particular interest for theoretical treatment because they have an equilibrium constant which is by definition unity. As part of our ongoing effort to study nonaqueous electron transfer by transition-metal complexes, we have chosen the chromium(0,I) hexakis(2,6-diisopropyl phenyl isocyanide), $Cr(CNdipp)_6^{0/+}$, system for detailed study. Several features of this class of complexes make them appealing for study. They are substitution inert in three oxidation states, (Cr(0,I,II)), crystal structures are known for the four oxidation states of $Cr(CNC_6H_5)^{0/+/2+/3+}$, a variety of symmetrical complexes can be synthesized that have adequate stability and solubility in nonaqueous solvents over a large temperature range, and the electron self-exchange process can be followed directly by ^1H NMR line broadening. The reactivity of the system studied here can be compared to that of the isoelectronic manganese(I,II) hexakis(isocyanide) electron self-exchange reactions studied previously.[4-6] Furthermore, in the $Cr(CNdipp)_6^{0/+}$ reaction there is no Coulombic repulsion between the reactants in forming the precursor complex. This work sets the reference point for further studies in which the $Cr(CNdipp)_6^{+/2+}$ exchange is being studied along with that of other aryl isocyanide ligands.

Experimental Section

The ligand 2,6-diisopropylphenyl isocyanide (CNdipp) was prepared from the corresponding aniline (Aldrich) by utilizing dichlorocarbene generated by a phase-transfer method.[7] The hexakis(2,6-diisopropylphenyl isocyanide)chromium(0) complex, $Cr(CNdipp)_6$, was synthesized from $Cr_2(CH_3CO_2)_4(H_2O)_2$ by a standard method[8] and recrystallized from a dichloromethane–hexane mixture under nitrogen to give bright red crystals. Anal. Calcd: C, 79.70; H, 8.74; N, 7.15. Found: C, 79.53; H, 8.73; N, 7.10. Characteristic infrared bands are $\nu_{C\equiv N}$ = 1959 cm^{-1} (broad) and a ring vibration at 1585 cm^{-1}. Hexakis(2,6-diisopropylphenyl isocyanide)chromium(I) tetrafluoroborate ($Cr(CNdipp)_6BF_4$) was prepared according to the method of Treichel and Essenmacher[9] except that $AgBF_4$ was used as the oxidant and the anion source. The complex was recrystallized from an acetone–hexane mixture to give bright yellow crystals. Anal. Calcd: C, 74.21; H, 8.14; N, 6.65; F, 6.02. Found: C, 73.12; H, 8.16; N, 6.49; F, 5.83. Characteristic infrared bands are $\nu_{C\equiv N}$ = 2060 (strong), 1432, and 1055 cm^{-1}. Tetrabutylammonium tetrafluoroborate (Bu_4NBF_4) was prepared as previously described.[10] Microanalysis was done by Galbraith Laboratories. Infrared spectra were collected by use of KBr pellets with a Perkin-Elmer 283-B instrument.

Methylene-d_2 chloride (MSD Isotopes, Merck) was degassed by three freeze–pump–thaw cycles and stored in an evacuated bulb, in the dark, until used. Samples were prepared by weighing the appropriate quantities of solid reagents into a 5-mm NMR tube (Wilmad Glass Co.) with a Teflon valve. The samples were placed on a vacuum line where methylene-d_2 chloride was vacuum transferred into the tube. The tubes were kept at −95 °C and in the dark until used. Concentrations were calculated from the weight of the solids and the weight of the solvent added to the NMR tube. The error in each weight is taken as 0.0001 g, giving a total concentration error of typically 3%.

Data were collected on a Nicolet NT200WB instrument operating at 200 MHz. Acquisition parameters were a 4.5-μs pulse width, a 500-μs postacquisition delay, a 4000-Hz sweep width, a 32K block size, and 256 pulses. To obtain accurate line widths, the field homogeneity was carefully adjusted for each spectrum on the basis of the amplitude of the ^2H lock signal and the free-induction decay signal. All samples were spun. The accumulation time at each temperature was 18 min.

Temperature was controlled with the built-in gas-flow temperature controller. Dry nitrogen flows through a coil immersed in liquid nitrogen. The accuracy of the control was checked by use of the method of Van Geet[11] as modified by Raiford et al.,[12] corrected to 200 MHz, by adding a sealed capillary of methanol to the experimental sample. The accuracy is ±1 °C and the precision is ±0.5 °C. The temperature range used, −89 to +22 °C, was dictated by the freezing point of the solvent and the lack of line broadening observed at higher temperatures.

The stability of the solutions at room temperature was determined by measuring the line width and shift and checking for any new peaks at various time intervals. Solutions of the Cr(I) complex were stable for days. Solutions of the Cr(0) complex, ca. 3 mM, showed some initial oxidation (≤1%) but were then stable for 8 h, after which they slowly decomposed. However, 40 mM solutions showed no evidence of oxidation and were stable for 10 h.

The exact chemical shift and widths for the Cr(0) and Cr(I) complexes were determined from pure solutions of each complex at each

(1) Marcus, R. A.; Sutin, N. *Biochim. Biophys. Acta* **1985**, *811*, 265.
(2) Newton, M. D.; Sutin, N. *Annu. Rev. Phys. Chem.* **1984**, *35*, 437.
(3) Nielson, R. M.; McManis, G. E.; Golovin, M. N.; Weaver, M. J. *J. Phys. Chem.* **1988**, *92*, 3441-3450.
(4) Nielson, R. M.; Wherland, S. *Inorg. Chem.* **1984**, *21*, 1338.
(5) Nielson, R. M.; Wherland, S. *J. Am. Chem. Soc.* **1985**, *107*, 1505.
(6) Nielson, R. M.; Wherland, S. *Inorg. Chem.* **1986**, *25*, 2437.
(7) Weber, W. P.; Gokel, G. W. *Tetrahedron Lett.* **1972**, *17*, 1637.
(8) Jolly, W. L. *The Synthesis and Characterization of Inorganic Compounds*; Prentice-Hall: Englewood Cliffs, NJ, 1970.
(9) Essenmacher, G. J.; Treichel, P. M. *Inorg. Chem.* **1977**, *16*, 800.
(10) Borchardt, D.; Pool, K.; Wherland, S. *Inorg. Chem.* **1982**, *21*, 93.
(11) Van Geet, A. L. *Anal. Chem.* **1970**, *42*, 679.
(12) Raiford, D. S.; Fisk, C. L.; Becker, E. D. *Anal. Chem.* **1979**, *51*, 2050.

0020-1669/89/1328-0601$01.50/0